Atom Indonesia

Journal homepage: https://atomindonesia.brin.go.id

Monte Carlo Evaluation of the Impact of Flattening Filter Removal and Collimator on the Energy Properties of a 6 MV Photon Beam Using GATE

I. Lagrini[1*], M. Bencheikh[1], I. Maouhoubi[2], A. Khallouqi[3], H. Sekkat[4], O. Berradi[5], M. Bougtib[6]

[1]*LSIB Laboratory, Faculty of Sciences and Technologies Mohammedia, Hassan II University of Casablanca, BP 146, Mohammedia 28806, Morocco*
[2]*Solid Physics Laboratory, Group of Nanomaterial and Renewable Energies, Department of Physics, Faculty of Sciences Dhar El Mahraz, Sidi Mohamed Ben Abdellah University, BP. 1796, Fez, Morocco*
[3]*Laboratory of Health Sciences and Technologies, Higher Institute of Health Sciences, Hassan 1st University, BP 539, Settat, Morocco*
[4]*Sciences and Engineering of Biomedicals, Biophysics and Health Laboratory, Higher Institute of Health Sciences, Hassan First University, Settat 26000, Morocco*
[5]*Laboratory of Applied Physics, Computer Science and Statistics, Faculty of Sciences Dhar El Mahraz, Sidi Mohamed Ben Abdellah University, BP. 1796, Fez, Morocco*
[6]*Department of Radiation Oncology, University Hassan II, Hospital of Fez, Fez, Morocco*

ARTICLE INFO

Article history:
Received 22 February 2025
Received in revised form 22 June 2025
Accepted 10 August 2025

Keywords:
Photon beam
Removing flattening filter
Monte carlo simulation
Gate/Geant4
Secondary particle production
Surface dose

ABSTRACT

This study aims to evaluate the impact of removing the Flattening Filter (FF) and the secondary collimator on the energetic properties of a 6 MV photon beam. The Monte Carlo (MC) simulation platform GATE/Geant4 (v9.3) was used to evaluate particle fluence, energy fluence distribution, and energy deposited at the phantom surface with a 10 × 10 cm² field size and a Source-to-Surface Distance (SSD) of 100 cm, as well as the production of secondary particles. Validation using Varian Phase-Space (PS) data showed excellent agreement, with gamma pass rates of 99% for Percentage Depth Dose (PDD) and 98% for lateral profiles at depths of 5 and 10 cm, based on a 2% - 2 mm gamma index criterion. Beam quality parameters ($TPR_{20/10}$) and Relative Dose Differences (RDD) confirmed a margin of error of less than 2%, validating the accuracy of the geometric simulation model. Removing the FF significantly increased the energy fluence of the particles responsible for energy deposition on the surface of the water phantom, increasing relatively by 136% for photons and 55% for electrons in the energy ranges of 0.49 - 0.525 MeV and 0.28 - 0.315 MeV, respectively. Moreover, the secondary collimator contributes significantly to the production of secondary particles that affect the dose distribution and beam energy properties.

INTRODUCTION

Radiotherapy remains one of the most effective cancer treatments, where precise radiation beams target tumor cells to limit damage to surrounding healthy tissue [1,2]. The use of Linear accelerators (Linac) plays a vital role in delivering precise radiation beams [3,4]. However, the configuration of the Linac system, such as the use of Flattening Filters (FF), can influence the dose distribution and overall treatment outcomes. Flattening filters are traditionally used to create a uniform dose profile [5,6], but recent advancements have introduced "Flattening Filter-Free" (FFF) beams, offering new possibilities in radiation delivery [5,7,8].

Flattening Filter-Free photon beams have gained significant attention in modern radiotherapy because they deliver faster dose rates while reducing radiation exposure to healthy tissues. By removing the flattening filter, FFF beams allow for increased peak dose intensity and decreased dose spread outside the target area, which enhances treatment outcomes in techniques such as Intensity-Modulated Radiation Therapy (IMRT), Image-Guided Adaptive

*Corresponding author.
E-mail address: ismail.lagrini1-etu@etu.univh2c.ma
DOI: https://doi.org/10.55981/aij.2026.1632

Radiation Therapy (IGAT), Stereotactic Body Radiation Therapy (SBRT), and Stereotactic Radio Surgery (SRS) [7,9-12]. However, the absence of the FF also alters particle production within the Linac system, particularly at the jaws and the Multi-Leaf Collimator (MLC), raising concerns about the impact of FFF beams on secondary particle production and overall dose distribution.

Monte Carlo (MC) simulations, a powerful tool for radiation transport analysis, are commonly used to study these complex interactions [13-16]. In this study, we employ the GATE code, a widely recognized MC simulation tool, to assess the effects of Linac configurations with and without FF [17]. The analysis focuses on the behavior of particle fluence through a water phantom, simulating the treatment environment. Understanding the particle behavior in both configurations is crucial for evaluating the impact on surface doses and overall treatment efficacy.

Benchiekh et al. (2017), employed an MC calculation method to model a Varian Clinac 2100 Linac, both with and without an FF, to assess the filter's effect on the energy properties of particles, including energy fluence, mean energy, and the energy fluence distribution at the phantom's surface [18]. Krim et al. (2021) proposed a precise simulation method aimed at minimizing particle interactions within X-ray beams generated by the Elekta accelerator, to enhance clinical performance and reduce unnecessary radiation exposure to patients [19]. Sigamani et al. (2016), conducted a detailed analysis of surface and buildup region doses for both Flat Beams (FB) and FFF beams using the Varian TrueBeam Linac [20]. Their results showed that FFF beams produced a significantly higher surface dose and were less sensitive to variations in the Source-to-Skin Distance (SSD) compared to flattened beams.

Additionally, The results of several previous studies conducted at different energies to evaluate the dosimetric and energy characteristics of a beam without an FF have shown that the use of a Linac without an FF can increase the efficiency of radiation dose delivery to the therapeutic target by minimizing the dose to healthy tissue [5,8,11,12,20-22]. However, the FFF configuration also leads to a significant increase in unwanted surface dose. These studies have often focused on comparing the effects of with or without an FF on surface dose alone, without considering the effects on the beam before it reaches the surface of the water phantom, especially the primary and secondary particles that play an important role in increasing the surface dose.

In the literature, MC simulation has been widely used in many studies to model the physical interactions of photons and electrons in the patient's body, making it an essential element in designing radiotherapy treatment plans [23]. However, despite significant advances in the modeling of Linacs, the precise effects of Linac head components on beam characteristics before they reach the patient are not yet fully understood or represented with sufficient accuracy in current models. The materials used in these components, such as the flattening filter, play a crucial role in shaping the beam, especially with respect to the production of scattered photons. Previous studies have shown that the nature, thickness, and arrangement of the material can significantly affect the off-axis radiation distribution [24].

Therefore, this study aims to assess the impact of the presence or absence of a Flattening Filter on the energy properties of a 6 MV photon beam, including particle fluence, energy fluence distribution, and secondary particle production. By analyzing these parameters, the aim is to enhance understanding of how Linac head components influence particle fluence and fluence energy distribution at the surface of a water phantom, while identifying the type of particles and their energy range that contribute directly to the undesirable surface dose.

METHODOLOGY

Varian phase space files

A direct and efficient simulation of a TrueBeam Linac (Varian Medical Systems, Palo Alto, CA) necessitates precise geometric details that are not publicly accessible due to their confidential nature. For researchers employing MC methods, Varian provides Phase-Space Files (PSF) compliant with IAEA standards, generated using Geant4 V4.9.2.p01 MC code [25]. These files are created from data collected on a plane situated just above the (X, Y) secondary collimators and encompass detailed information such as the position, direction, energy, and type of each particle [26]. Their validity has been confirmed in several previous studies utilizing Geant4 [27], EGSnrc [28], and PRIMO [29], demonstrating their capability to reproduce dose distribution curves (PDDs) accurately, therefore establishing them as reliable references for advanced MC simulations.

In this study, TrueBeam PSF (version 2) was used, containing 46×10^6 particles for the X6MV-FF and 47×10^6 particles for the X6MV-FFF recorded at a distance of 26.70 cm from the target. These files were downloaded from the database provided by Varian [25]. The PSF was then propagated downstream using the TrueBeam-STx Linac geometry.

Code and software used for the Monte Carlo simulation

The simulation used version 9.3 of GATE (Geant4 Application for Tomographic Emission) on an Ubuntu LTS 20.04 for its ability to accurately represent radiation interactions with different materials, allowing for accurate and detailed results [30]. The open-source GATE software was developed to simulate the transport and interaction of photons, hadrons, and electrons in various environments [31]. The OpenGATE collaboration facilitated its development, and it relies on the Geant4 toolkit, which offers advanced functionalities for complex radiation transport simulations.

To maintain and analyze the input and output information from the simulations, ROOT version 6.30, an object-oriented data analysis framework, was employed [32]. Graphical user interfaces were utilized to visualize and verify the geometry of components by executing GATE in QT mode (Geant4 QT User Interface) [19,33]. This approach enabled precise control over simulation parameters and ensured accurate representation of the modeled systems.

TrueBeam representative beam data

According to the TG-106 report from the American Association of Medical Physicists (AAPM), it is essential to utilize Golden Beam Data (GBD) to evaluate the accuracy and efficacy of Linac beam measurements [34]. These data serve as a reference based on average measurements taken from various Linacs worldwide. The GBD provides precise information regarding beam properties such as dose profiles, beam energies, and output factors supplied by manufacturers. These data are crucial to ensure device performance meets clinical standards [35]. The results obtained in this study were compared with the GBD to ensure the accuracy of the simulation parameters. The required information for the mentioned purpose was extracted from the Varian database.

Simulation of particle interaction processes

To execute an accurate simulation of any system, it is imperative to simulate all physical particles (events) within the logical volume to reflect real-world occurrences [19]. In the simulation framework of this study, both primary and secondary particles generated within the Linac system span a range of megavolt energies. Consequently, standard electromagnetic interaction models and standard electromagnetic-type option-3 were employed to ensure simulation accuracy [17]. These models facilitate precise simulation of scattering, absorption, and secondary particle production, which are essential for obtaining reliable radiation dose simulations.

Geometry of the linac setup

The geometry of the TrueBeam Linac used in this study was carefully simulated using the GATE code to ensure maximum accuracy. This setup includes several critical components, detailed in Fig. 1. First, the Varian PSF, located directly above the jaws at 26.70 cm, captures data from millions of particles. This phase space simulation is independent of patient-specific parameters and is based on manufacturer-provided specifications, employing the Geant4 MC code. Below this is the jaw assembly, modeled as a 78 mm thick tungsten alloy cube, allowing precise radiation field definition by adjusting along the X and Y axes to reduce unwanted particles outside the field. Positioned just below the X-axis jaw at 0.9 cm is the Multi-Leaf Collimator (MLC), specifically the 120-leaf Millennium MLC. This collimator consists of two blocks, each 6.7 cm thick, containing 60 independent tungsten leaves: 40 internal leaves with a width of 0.5 cm and 20 external leaves measuring 1 cm, all spaced 0.005 cm apart and oriented along the Y-axis. This configuration allows for precise beam shaping to conform to target geometry, enhancing treatment efficacy. Finally, a 60 x 60 x 40 cm^3 cubic water phantom was used, with its upper face iso-centered at SSD = 100 cm, serving as a reference medium for dose measurements and quality assurance in the simulation.

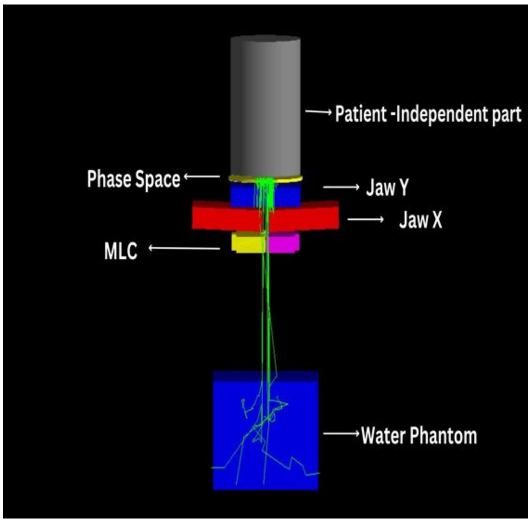

Fig. 1. Geometric description of Linac head, including the position of the phase space above the jaws (X, Y) on Gate v9.3.

Simulation strategy

The simulation strategy in this study consisted of three primary steps. First, the phase space was defined below the MLC, capturing the particulate fluence distribution of leakage particles for a photon beam with and without an FF. This PSF is essential for analyzing leakage particle distribution before interacting with other Linac head components. Both PSFs were positioned at SSD of 100 cm, allowing one to assess the impact of leakage particles on surface dose at the phantom level and to verify the Linac geometric configuration, ensuring accuracy under the specified simulation conditions. The second step involved the use of actors and specialized tools within GATE, that enable data collection and interaction within simulations [17]. For precise dosimetric analysis, the DoseActor was utilized to obtain parameters such as PDD and lateral dose profiles in a water phantom, with voxel sizes set to 5 x 5 x 2 mm^3, 2 x 5 x 5 mm^3, and 5 x 2 x 5 mm^3, respectively. All dose profiles calculated using GATE were normalized to the maximum dose point d_{max}(cm) and compared with measured data. To assure time-saving computation and reduce processing time, the KillActor was used with energy cut-off values of 0.01 MeV and 0.7 MeV for photons and electrons, respectively. Additional particle fluence and energy spectrum actors were deployed to quantify particle numbers passing through phantom surfaces and to assess the energy spectra deposited on these surfaces, offering insights into the particles' impact on therapeutic quality and dose distribution at the surface. The third step involved clustering and CPU timing, where a parallel processing approach using SLURM was implemented in partnership with CNRST Morocco's team. This cluster computing method was applied to achieve the desired uncertainty levels efficiently, enhancing simulation performance.

Calculation and validation of dosimetric parameters

To evaluate the beam quality, parameters such as the Tissue-Phantom Ratio ($TPR_{(20/10)}$), the depth of maximum dose d_{max}(cm), the depth at half-dose d_{50}(%), and the dose at 10% depth D_{10}(%), as defined in the IAEA TRS-398 standard, were calculated and compared with the measured values.

In radiotherapy, the parameter $TPR_{(20/10)}$ is used to express the beam quality index of high-energy photon beams. [36]. $TPR_{(20/10)}$ is the ratio between the absorbed doses at depths of 20 cm and 10 cm, measured in a water phantom for a reference square field of 10 × 10 cm² with an SSD of 100 cm. The $TPR_{(20/10)}$ can be calculated empirically using the following Eq. (1).

$$TPR_{20/10} = 1.2661 \times PDD_{20/10} - 0.0595 \quad (1)$$

Additionally, $PDD_{(20/10)}$ is the ratio of PDDs at depths of 20 cm and 10 cm under the same measurement conditions. The difference between measured (Dm) and calculated (Dc) doses at each point of the dose depth curves (PDD) or lateral profiles was evaluated by the Relative Dose Difference (RDD) [37]. The relative error rate (RDD) is expressed as a percentage and calculated according to the following formula, as presented in Eq. (2).

$$RDD(\%) = \frac{|Dm - Dc|}{Dm} * 100 \quad (2)$$

In addition, the gamma index (γ) was used as a comparison tool to assess the agreement between calculated and measured dose distributions [38]. In this study, the tolerance criterion is 2% - 2 mm, meaning that a point is valid if it respects a dose difference of less than 2% and a distance of less than 2 mm from the reference points. The gamma index is calculated from the following Eq. (3).

$$\gamma = min\left(\sqrt{\left(\frac{\Delta D}{\Delta D_{max}}\right)^2 + \left(\frac{\Delta r}{\mathrm{DTA}}\right)^2}\right) \quad (3)$$

The spatial separation between the evaluation point (r_c) and the reference point (r_m) is represented by the distance Δr. ΔD is the dose difference between these two points. The dose tolerance criterion is ΔD_{max}, and the distance tolerance limit is DTA. If $\gamma > 1$, the deviation is greater than the specified tolerance limits; if $\gamma < 1$, the deviation is within the permitted limits.

Briefly, this study aims to validate the use of Varian PSF for the MC simulation of a TrueBeam Linac using the GATE/Geant4 code, with validation for a 10 × 10 cm² field at SSD = 100 cm for both 6 MV photon beams FF and FFF. It also investigates the impact of removing the flattening filter, as well as the secondary collimator (MLC and Jaws XY), on the energetic properties of the 6 MV photon beam and on the production of contaminating secondary particles. Additionally, we also determined the difference in the energy flux of the particles contributing most to the dose increase at the phantom surface at SSD = 100 cm for a field of 10 x 10 cm^2, the local difference was determined as follows, Eq. (4).

$$Local\ difference\ (\%) = 100 * \frac{(X_{FFF} - X_{FF})}{X_{FF}} \quad (4)$$

Where, X_{FFF} defines as energy fluence of particles with the same amount of energy at the surface of the phantom in FFF mode; whereas X_{FF} defines as energy fluence of particles with the same amount of energy at the surface of the phantom in FF mode.

RESULTS AND DISCUSSION

The findings in this paper are based on MC simulations of a TrueBeam Linac with a nominal energy of 6 MV. Two modes, FF and FFF photon beams, were simulated using a Varian PSF. The simulations were carried out with an SSD of 100 cm and a field size of 10 × 10 cm². Subsequently, the MC simulation and beam quality were verified by comparing these results with the measured data provided by the manufacturer.

Beam quality index validation

Table 1 illustrates the good agreement between the GATE simulations and the experiment results (Measured data), with slight differences in the beam quality parameters. The differences for $TPR_{(20/10)}$ showed that the accuracy was high, particularly for FFF mode, with 0.82% for FF mode and 0.39% for FFF mode. The variances for D_{10}(%) were smaller than 1%, while the differences for d_{max}(cm) were less than 3 mm with a relative variation of less than 1%. These findings are consistent with the IAEA's beam verification recommendations (TRS-398). These metrics demonstrate the GATE simulator's dependability in treatment planning and beam verification in radiotherapy by confirming that they provide precise dose estimations.

Comparison of depth dose characteristics

The PDDs obtained by MC simulations for the photon beam, with and without FF, for a field size of 10 × 10 cm², with an energy of 6 MV and a source-to-surface distance of 100 cm, were compared with measured data. The comparison between simulated and measured depth dose profiles for the FF photon mode is shown in Fig. 2 (a). The simulated and measured curves are in overall agreement, with a difference of 1 mm at the maximum dose depth d_{max}(cm). According to the results of the gamma index distribution for the FF photon mode, shown in Fig. 2 (b), more than 99% and 95% of the points meet the acceptability criteria of (2% - 2 mm) and the stricter criterion of (1% - 1 mm), respectively, with a value of less than 1. This confirms that the simulation results are generally in good agreement with the measurements, especially in critical areas (build-up area and around the D_{max}).

For the FFF photon mode, as shown in Fig. 2 (c), the comparison of the PDDs showed a good overall correspondence, but the deviations were slightly larger, reaching 2 mm at D_{max}. The absence of a flattening filter in FFF mode resulted in a more complex beam distribution, which may explain these differences. The gamma index for the FFF photon mode shown in Fig. 2 (d) revealed that 99% and 94% of the points meet the acceptability criteria of (2% - 2 mm) and the stricter criterion of (1% - 1 mm), respectively, with a value of less than 1. This indicates that the simulation is generally in good agreement with the measurements.

Figure 3 shows the depth relative dose difference RDD (%) for both FF and FFF modes. In critical areas (build-up and around the D_{max}), the average error was below 0.5% for both FF and FFF modes. A slight increase in the gap for the FFF mode in the build-up area may be related to the lack of a flattening filter, resulting in a more complex, concentrated, and non-homogeneous beam distribution, making modeling with absolute accuracy more difficult. However, the increase in error, of about 1.5% on average, at depths greater than 15 cm for both the FF and FFF modes was notable. For the FF mode, the deviations became larger beyond 25 cm, which can be attributed to the complexity of the beam and the increase in secondary particle interactions, which are more difficult to simulate accurately.

Table 1. Comparison of calculated and measured beam quality index parameters for the X6-MV FF and FFF photon beam modes.

Parameters	Photon beam	Gate	Measured data	Error estimation	
$TPR_{(20/10)}$	FF	0.675146	0.666982	0.82%	
	FFF	0.636202	0.632368	0.39%	
d_{max}[cm]	FF	1.4	1.5	1 mm	< 3 mm
	FFF	1.4	1.2	2 mm	
D_{10}(%)	FF	0.663	0.664	0.1%	
	FFF	0.629	0.635	0.55%	
d_{50}[cm]	FF	15.4	15.1	3 mm	< 3 mm
	FFF	13.8	14	2 mm	

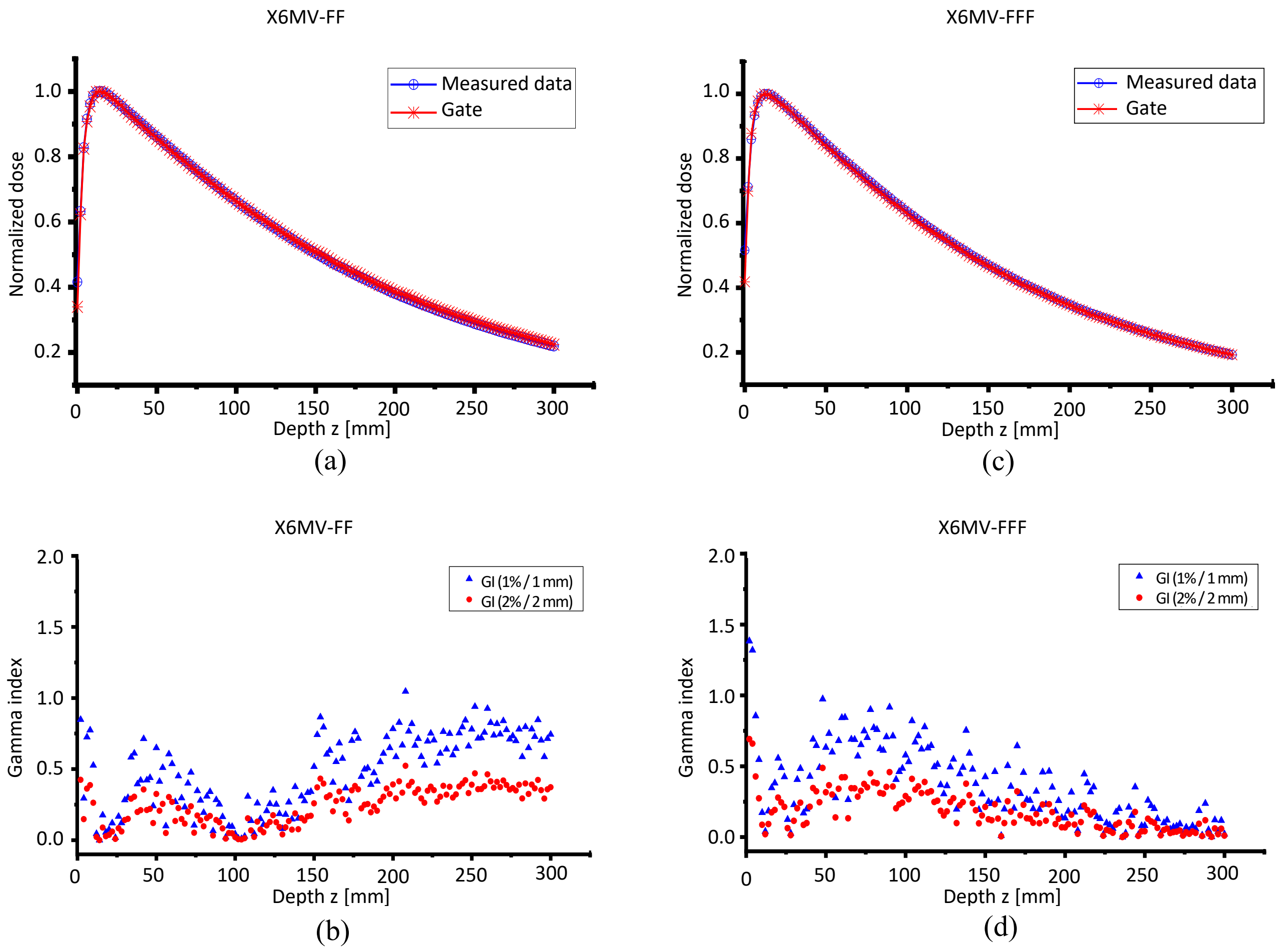

Fig. 2. Comparison of simulated and measured PDDs for X6MV-FF and FFF photon beam modes with a 10 × 10 cm² field size at SSD 100 cm, Including gamma index Analysis between simulated and measured PDDs.

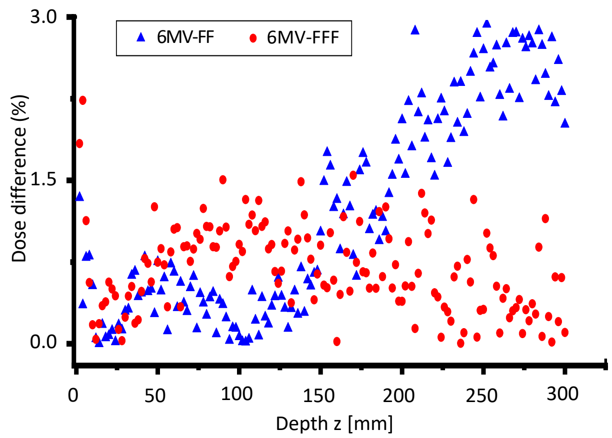

Fig. 3. Dose difference between simulated and measured PDD for a 10x10 cm² field size SSD 100cm in X6MV-FF and FFF modes.

According to the results, the MC simulation approach can accurately predict depth dose distributions for FF and FFF photon beams, with minor deviations that we interpreted as consequences of beam complexity and experimental limitations.

Comparison of dose profile characteristics

The lateral dose profiles obtained show that MC simulations accurately represent dose distributions, with notable variations depending on the beam configuration. For the FF photon beam mode, Fig. 4 (a) presents the comparison between the simulated lateral dose profiles measured at a depth of Z = 10 cm, as well as their gamma index distribution, while Fig. 4 (b) shows these profiles at Z = 5 cm. The measured profiles show excellent agreement with the measurements, with over 98% of the points meeting 2% - 2 mm criterion and an average value gamma index below 1. This indicates very good dose simulation accuracy, both in the area of the central axis of the beam and outside the field. In the penumbral zone characterized by a rapid decrease in dose, the differences between the simulated and measured dose distributions were slightly more pronounced. This difference was due to the rapid drop in dose in this area, which resulted in a strong dose gradient and may be related to the conditions of the measurements, in particular, the size of the active volume of the ionization chamber used.

Figures 4 (c) and (d) compare the side profiles for the FFF mode and their gamma index at Z = 10 cm and Z = 5 cm, respectively. The dose profiles at Z = 10 cm and Z = 5 cm also show good agreement with the measurements, with approximately 98% of the points meeting the 2% - 2mm gamma index criterion in the central region, with a mean value of less than 1.

The deviations were slightly larger in the penumbra area due to the absence of a flattening filter. In addition to previous analyses, the absence of this filter resulted in a more concentrated and less homogeneous beam distribution, which affecting the accurate simulation of dose distribution in this region.

The analysis of the dose profile shows excellent agreement between the MC simulation results and the experimental measurements, with more than 98% of the points meeting the 2% - 2 mm criterion in the FF and FFF photon beam modes.

These results reflect the accuracy of the modeling of dose distribution in central and out-of-field regions, with some difficulties in the penumbral region, but which remain within acceptable limits.

In general, the results obtained using the Monte Carlo GATE code showed good agreement between calculated and measured dose profiles, as well as beam quality parameters. Using the gamma index criteria (1% - 1 mm) and (2% - 2 mm) to assess dose accuracy, our results are in line with IAEA recommendations. In addition, the values we obtained for beam quality parameters such as D_{max}, D_{10}(%), and $TPR_{(20/10)}$ are in good agreement with those obtained in previous studies [5,8,10,33].

When comparing our results with those of these studies, slight differences were observed in terms of maximum dose and dose distribution in the shadow zone, which can be explained by the simulation conditions and limitations of MC simulations, particularly in heterogeneous structures. These results confirm that GATE simulation is a reliable tool for predicting dose distribution with high accuracy in different clinical contexts.

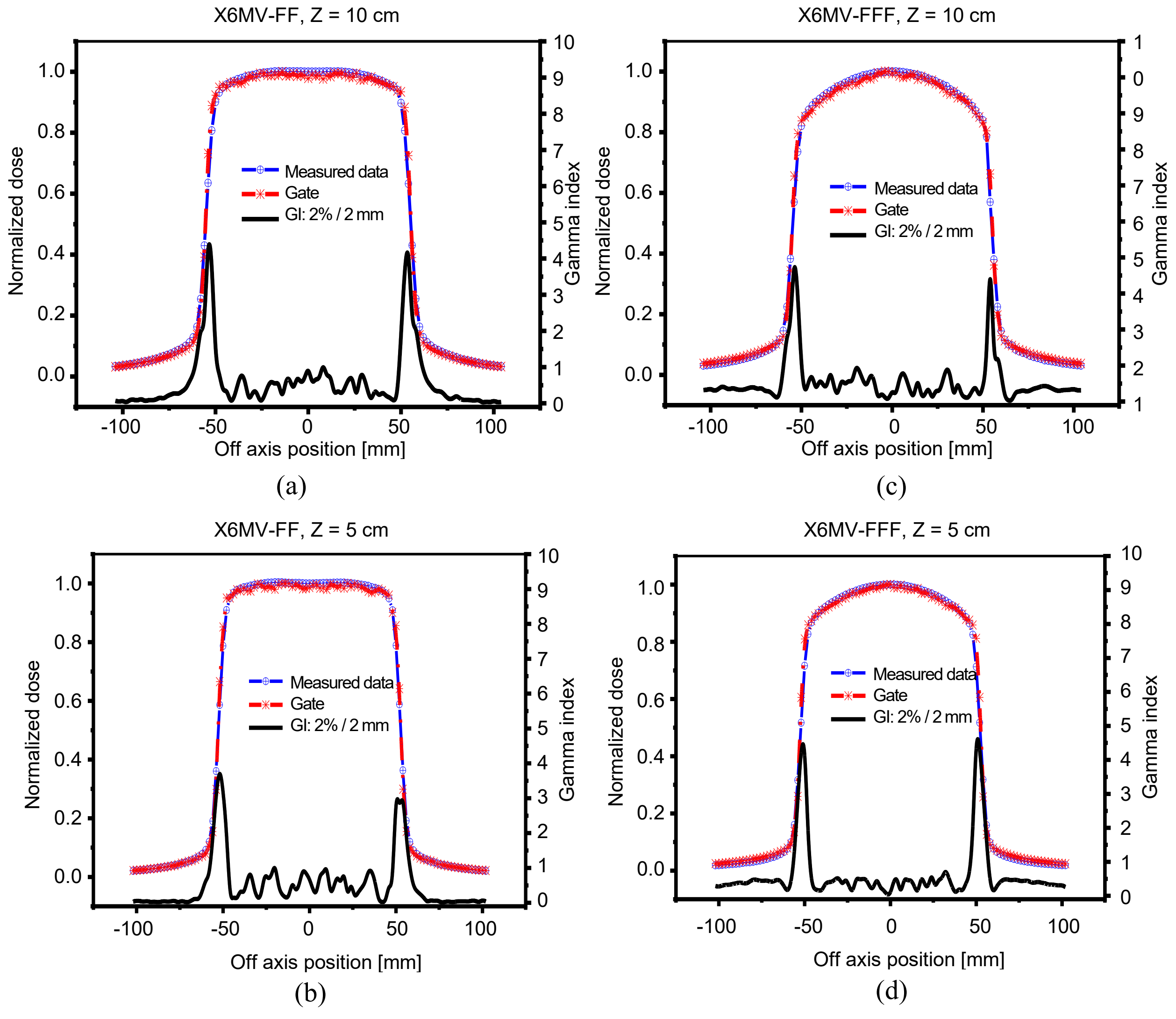

Fig. 4. Comparison of simulated and measured dose profiles at depths of 5 cm and 10 cm for a 10 × 10 cm² field at SSD 100 cm in X6MV-FF and FFF photon beam modes, including gamma analysis.

Track length and secondary production

Figures 5 (a) and (b) show the comparison between the free track length of particles before their interaction with matter for the FF and FFF photon beams, calculated by the Track Length Actor parameter. According to Fig. 5 (a), for both modes, the number of photons with a track length between 20 mm and 100 mm was more significant than those with a track length between 0 and 20 mm, as well as between 110 mm and 200 mm. In FFF mode, the photon flux with a track length of 0 to 10 mm was higher than in FF mode. This is due to the absence of a flattening filter in FFF mode, which allows the photons to travel without significant energy loss or flux reduction. In this case, a large number of photons mainly interact with the Y jaws, which are located directly beneath the source. Beyond 10 mm, an inversion was observed: the photon flux became more significant in FF mode. This inversion is due to the filter in FF mode, which redistributes energy and increases their probability of interacting with the X jaws and the MLC. Consequently, the photon flux in FFF mode is more concentrated at short distances, while FF mode promotes a more sustained flux through the secondary collimators, particularly the X jaws and MLC.

The track length of charged particles, such as electrons and positrons, is shown in this simulation. According to the results in Fig. 5 (b), a large number of charged particles had a free track length of between 0 and 1.4 mm. However, a small number of electrons had a trajectory length between 20 and 30 mm. In both modes, a large number of electrons had a free path length between 0 and 1.4 mm. However, in FFF mode, the electron flux was greater in this range. This is because more electrons interact with the Y jaw in FFF mode. This difference is due to the absence of the flattening filter, which allows a greater number of electrons to retain their energy and interact more rapidly with the secondary collimator components.

The secondary production actor allows us to quantify the secondary particles created by the interaction of primary particles in the simulation volume. According to Fig. 6, the number of electrons produced are similar in the X6-FF and X6-FFF modes, suggesting a stabilization of the quantity produced. However, the FF mode generated more photons and positrons than the FFF mode, even though the difference in positron numbers was small. It is possible that the FF mode, with its smoother beam profile, favors reactions generating secondary particles.

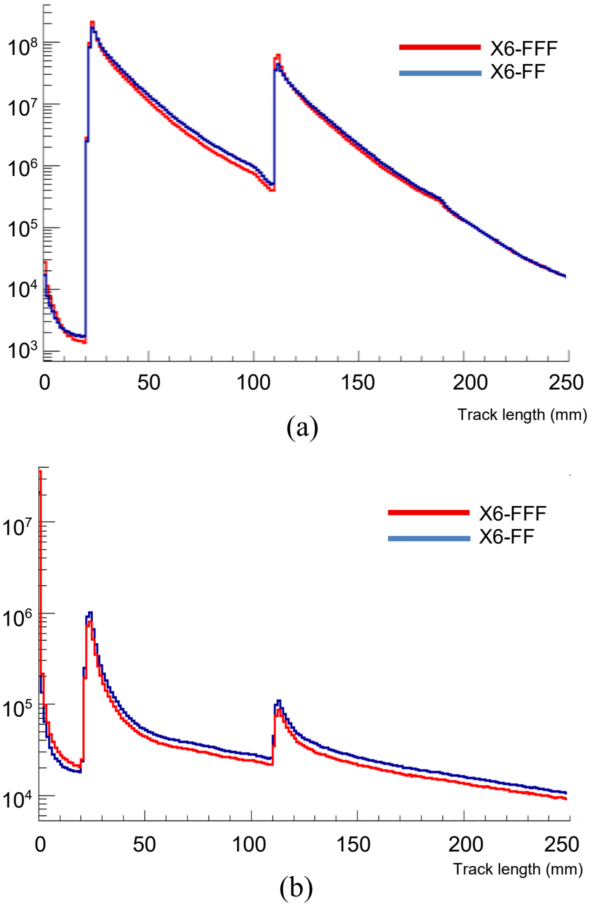

Fig. 5. Comparison between track lengths associated with (a) photon; (b) electron, and positron simulation for X6-FF and X6-FFF modes, using the track length actor.

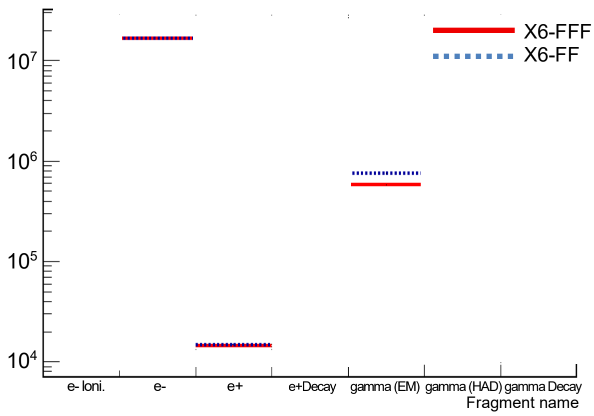

Fig. 6. Fragment production comparison for photons, electrons, and positrons in X6-FF and X6-FFF photon beam modes.

Our results concerning track length calculations and secondary particle production for the FF mode are in good agreement with Krim et al. (2021), as the results showed that photons and electrons with track lengths between 26 mm, 60 mm, 0 mm and 10 mm, respectively, are the most important component in interactions with the MLC in the Elekta Linac [19]. What distinguishes our study is its focus on the effect of the absence of the flattening filter in FFF mode, which leads to greater photon flux and focus at small distances, as well as increased electron interaction with the Y jaw.

On the other hand, electrons still comprise the vast majority of secondary production inside the Linac in both modes, with a notable increase for photons in FFF mode. This distinction makes it possible to analyze in detail the difference between the two modes in terms of particle interactions and fluxes, which contribute directly to the energy distribution.

Phase space analysis of secondary collimator leakage particles

The analysis of the phase space under the Multi-Leaf Collimators (MLC) allows for the collection of crucial information regarding leakage particles and thus provides a direct view of the interactions between the particles produced during treatment. Figure 7 illustrates the distributions of photons, electrons, and positrons leaking between the leaves of the MLC in the X6-FF and X6-FFF photon beam modes.

According to Figs. 7 (a) and (b), the results obtained showed that photons were the most frequent particles leaking from the MLC leaves, while electrons and positrons exhibited lower leakage rates, as demonstrated in Figs. 7 (c) and (d). This observation can be explained by the nature of photon interactions with matter, which allows for a large number of interactions before they are stopped. In contrast, electrons and positrons, due to their electric charge, interact more quickly with the MLC leaves, resulting in a reduction in their number compared to photons in both the X6-FF and X6-FFF modes.

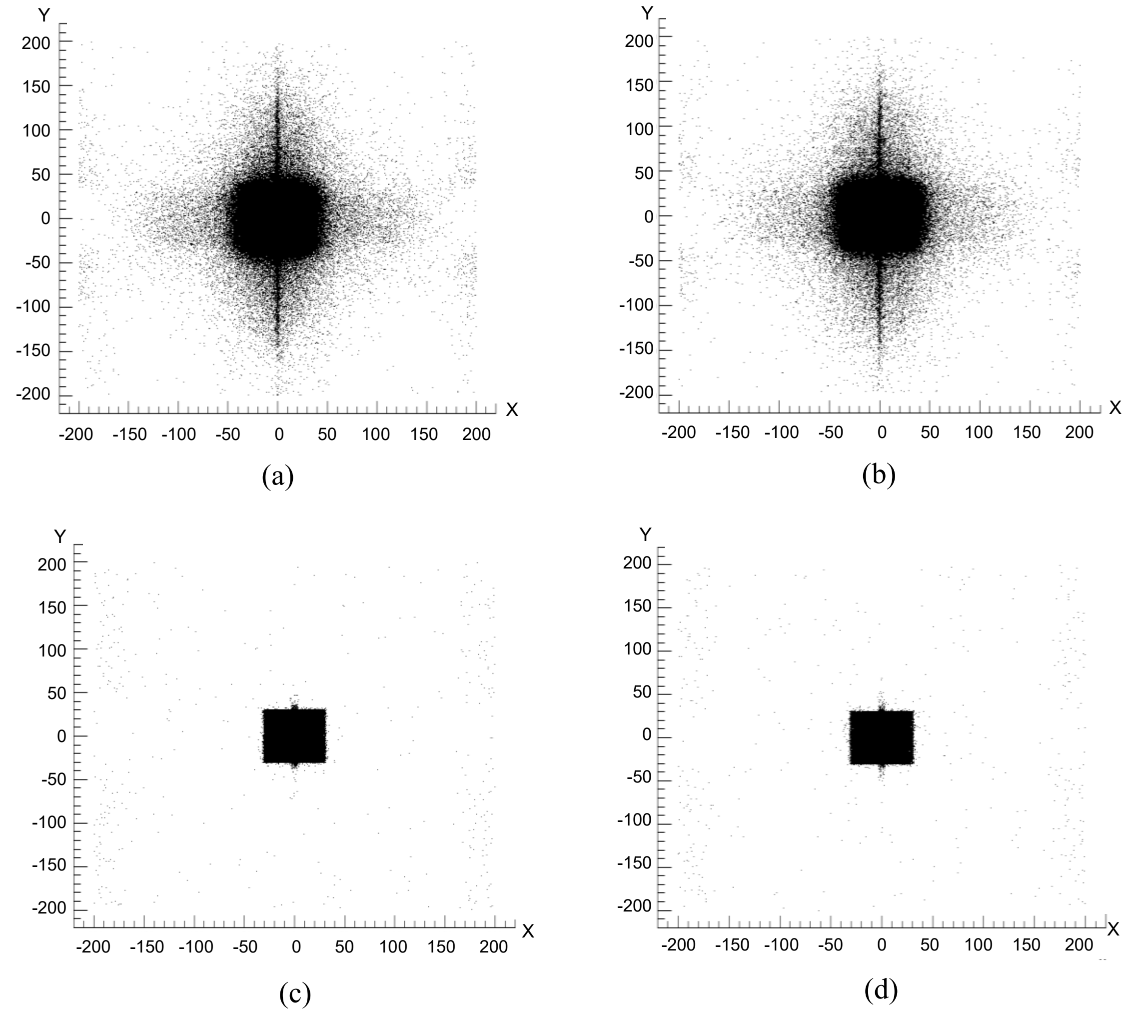

Fig. 7. Distribution of leakage photons (a and b) and leakage electrons and positrons (c and d) in X6-FF and X6-FFF modes, respectively, in the (X-Y) plane directly below the MLC.

Figure 8 shows a comparison of photon fluence at the phantom surface for the two modes, X6-FF and X6-FFF. The results showed a notable difference: in the X6-FFF mode, the absence of an FF resulted in higher photon fluence along the beam's main axis, with a rapid decrease away from this axis.

Conversely, the X6-FF mode produceed lower fluence at the center, but more uniform fluence along the X axis.

The comparison of electron fluence in FF and FFF modes is illustrated in Fig. 9 (a). The results revealed a significant difference in electron flux between the two modes. The electron fluence was higher in FFF mode, primarily due to the absence of a filter, which may allow more electrons to reach the surface of the phantom. Additionally, this increase in fluence in FFF mode could also be attributed to secondary electrons generated by low-energy photons near the surface of the water phantom. Despite this difference, the decrease in electron fluence off-axis is similar for both modes, indicating that the processes by which electrons interact with matter follow comparable physical principles.

According to Fig. 9 (b), the results showed an opposite trend regarding positron fluence between FF and FFF modes. Contrasting electrons, which showed higher fluence in FFF mode, positrons exhibit slightly higher fluence in FF mode. This can be attributed to the effect of the filter, which promotes the interactions necessary for positron formation. Information from the secondary production actor, illustrated in Fig. 6, further confirms that the number of positrons produced in the volume of interest is slightly higher in FF mode.

In terms of the energy deposition distribution by particles at the surface of the phantom, the results showed significant differences between the FFF and FF photon beam modes. According to Figs. 10 (a) and 10 (b), the number of photons and electrons interacting with the phantom's surface in FFF mode was higher compared to FF mode, particularly in the low-energy range, below 1 MeV. The maximum energy flux of the particles depositing the most energy on the phantom surface revealed a relative difference of 136% for photons between 0.49 and 0.525 MeV energy range, and 55% for electrons between 0.28 to 0.315 MeV energy range.

This difference is directly related to the absence of the FF, which leads to an increased fluence of low-energy photons at the phantom's surface, as well as an increased production of secondary electrons near the surface. Subsequently, the photon and electron fluxes gradually decrease in the higher energy ranges, and the energy deposition becomes nearly similar for energies above 3 MeV for photons and 1.5 MeV for electrons. Conversely, Fig. 10 (c) reveals an opposite behavior for positrons. There were slightly more positrons interacting with the phantom's surface in FF mode than in FFF mode. This difference is primarily due to the presence of the filter, which flattens the beam, allowing a high number of energetic photons to interact with the edges of the secondary collimator.

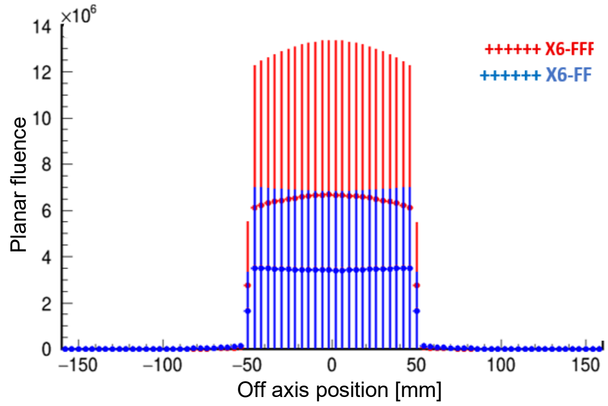

Fig. 8. Comparison of photon fluence in X6-FF and X6-FFF modes at the phantom surface for a 10 × 10 cm² field size SSD 100 cm.

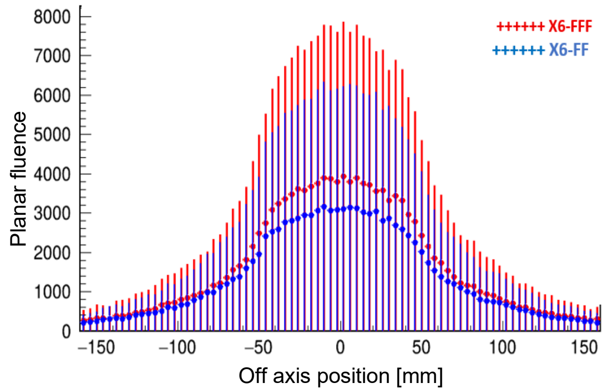

(a)

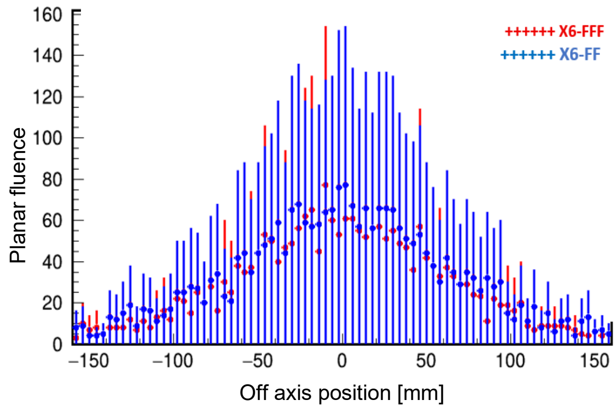

(b)

Fig. 9. Comparison of (a) electron fluence and (b) positron fluence in X6-FF and X6-FFF modes at the phantom surface for a 10 × 10 cm² field size SSD 100 cm.

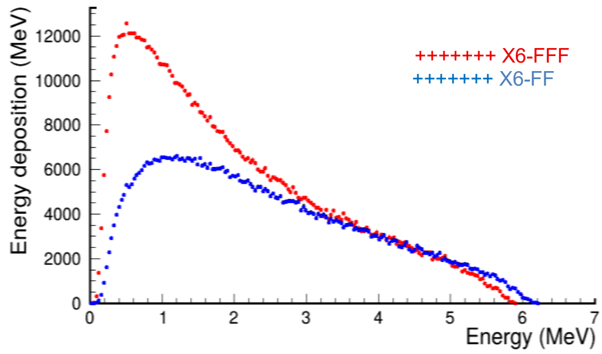

(a)

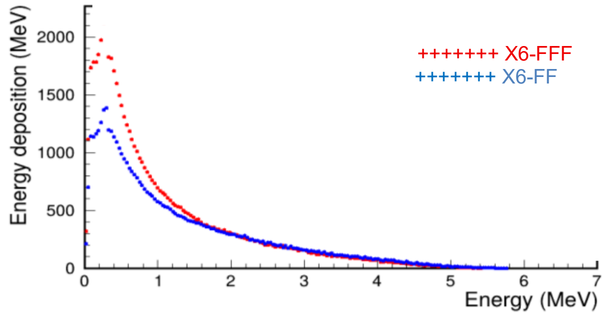

(b)

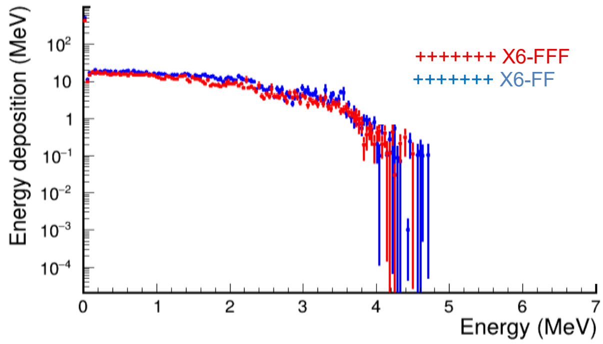

(c)

Fig. 10. Energy deposition spectra comparison for photons, electrons, and positrons at the phantom surface in X6-FF and X6-FFF modes for a 10 × 10 cm² field size SSD 100 cm; (a), (b), and (c) respectively.

This results in increased production of secondary positrons in that area. In FFF mode, the beam is less uniform, resulting in a different energy distribution of the beam, with a more concentrated intensity at the center. This decreases the number of photons interacting with the edges of the secondary collimator and jaws, reducing the photon-matter interactions that create electron-positron pairs.

Our results are consistent with previous studies that reported that using the FFF photon beam technique improves the efficiency of radiation dose delivery to the tumor, protects healthy tissue, and reduces treatment time. Furthermore, our results showed that the secondary collimator contributes significantly to the production of secondary particles and that removing the filter resulted in a significant increase in the energy fluence of the most energetic particles deposited on the surface of the water phantom. For positrons, the energy deposited on the surface was found to be almost identical in the FF and FFF modes. These results highlight the significant effect of filter removal on energy fluence and deposition, prompting further studies to understand the impact of radiation system design on efficiency and energy distribution.

CONCLUSION

In this study, the MC code GATE Version 9.3 was used to evaluate the effect of the secondary collimator and the absence of a filter on the energy characteristics of a 6 MV photon beam. Using phase space data extracted from the Varian platform, the accuracy of the linear accelerator simulation results, both with and without an FF, was verified by comparing depth dose curves to experimental data, achieving a strong 99% agreement. An agreement of 98% was also found when comparing dose profiles using the Gamma index with a 2% - 2 mm criterion.

These results confirm the reliability and accuracy of the simulation model used to study dose distribution and the effect of Linac head components on the energy characteristics of the photon beam.

The simulation results demonstrate that removing the filter in the FFF photon beam leads to a significant increase in the dose rate, but also causes fundamental changes in the particle fluence and energy distribution. This leads to contamination of the beam with secondary particles such as electrons and positrons and an increase in photon flux, especially in the low-energy range (<1 MeV). The study showed that the maximum energy flux of the particles responsible for energy deposition on the surface of the water phantom experienced a relative increase of 136% for photons in the (0.49 - 0.525) MeV energy range, and 55% for electrons in the (0.28 - 0.315) MeV energy range. Consequently, this results in a higher unwanted surface dose compared to the situation with the FF. On the other hand, the secondary collimator plays a critical role in shaping the radiation beam, influencing the energy spectrum and dose distribution. In general, the use of a Linac without an FF improves dose delivery efficiency while reducing the dose to healthy tissues compared to the conventional filtered beam. However, the use of the FFF mode requires a balanced approach to treatment planning.

ACKNOWLEDGMENT

As authors, we thank Varian Medical Systems for providing us with the phase space data from the Varian TrueBeam and allowing us to study the Varian linear accelerator technology and participate in its future development. We also greatly appreciate the Marwan HPC Center's support in performing the calculations for the complex simulations. Their contribution was essential to the completion of this research.

AUTHOR CONTRIBUTION

I. Lagrini contributed to the simulation and data analysis and was the lead author of the manuscript. M. Bencheikh was responsible for collecting the data necessary to validate the geometric simulation. I. Maouhoubi, A. Khallouqi, H. Sekkat, O. Berradi, and M. Bougtib provided guidance and suggestions to improve the manuscript, and they also reviewed the final manuscript to ensure its quality and accuracy.

REFERENCES

1. C. Allen, S. Her, and D. A. Jaffray, Adv. Drug Delivery Rev. **109** (2017) 1.
2. O. A. Firmansyah, A. F. Firmansyah, S. I. Sunaryati *et al.,* Atom Indones. **47** (2021) 181.
3. R. Sapundani, R. Ekawati, and K. M. Wibowo, Atom Indones. **47** (2021) 199.
4. M. Bencheikh, A. Maghnouj, J. Tajmouati *et al.,* Phys. Part. Nucl. Lett. **14** (2017) 780.
5. F. Haryanto, M. F. Rhani, C. Anam *et al.,* Atom Indones. **48** (2022) 147.
6. M. Mohammed, E. Chakir, H. Boukhal *et al.,* J. King Saud Univ. Sci. **29** (2017) 371.
7. A. Mesbahi, Appl. Radiat. Isot. **65** (2007) 1029.
8. R. Shende, S. J. Dhoble, and G. Gupta, Radiat. Phys. Chem. **199** (2022) 110339.
9. W. Purwati, F. Suhaimi, W. E. Wibowo *et al.,* Atom Indones. **49** (2023) 27.
10. A. Pichandi, K. M. Ganesh, A. Jerin *et al.,* Rep. Pract. Oncol. Radiother. **19** (2014) 322.
11. S. Sangeetha and C. S. Sureka, Radiat. Phys. Chem. **135** (2017) 63.
12. M. A. Najem, N. M. Spyrou, Z. Podolyák *et al.,* Radiat. Phys. Chem. **95** (2014) 205.
13. P. H. Lam, P. T. Dung, and P. Q. Trung, Atom Indones. **50** (2024) 221.
14. D. van Eeden and F. C. P. du Plessis, Radiat. Phys. Chem. **226** (2025) 112359.
15. I. F. Maulana, S. Yani, T. Sumaryada *et al.,* Radiat. Phys. Chem. **210** (2023) 111018.
16. G. R. Sunaryo, M. Jintana, and J. P. J. Gerin, Atom Indones. **37** (2011) 29.
17. S. Jan, D. Benoit, E. Becheva *et al.,* Phys. Med. Biol. **56** (2004) 4543.
18. M. Bencheikh, A. Maghnouj, and J. Tajmouati, Phys. Part. Nucl. Lett. **14** (2017) 953.
19. D. Krim, D. Bakari, M. Zerfaoui *et al.,* Rep. Pract. Oncol. Radiother. **26** (2021) 928.
20. A. Sigamani, A. Nambiraj, G. Yadav *et al.*, J. Med. Phys. **41** (2016) 85.
21. D. Georg, T. Knöös, and B. McClean, Med. Phys. **38** (2011) 1280.
22. G. Kragl, S. Wetterstedt, B. Knäusl *et al.,* Radiother. Oncol. **93** (2009) 141.
23. F. Kurniati, F. P. Krisna, J. Junios *et al.,* Atom Indones. **47** (2021) 205.
24. M. Bencheikh, A. Maghnouj, J. Tajmouati *et al.,* Moscow Univ. Phys. Bull. **73** (2018) 520.
25. M. Constantin, J. Perl, T. LoSasso *et al.,* Med. Phys. **38** (2011) 4018.
26. L. Grevillot, T. Frisson, D. Maneval *et al.,* Phys. Med. Biol. **56** (2011) 903.
27. P. Kandlakunta, S. Momin, A. Sloop *et al.,* Physica Med. **59** (2019) 1.
28. A. M. Bergman, E. Gete, C. Duzenli *et al.,* J. Appl. Clin. Med. Phys. **15** (2014) 148.
29. M. A. Efendi, A. Funsian, T. Chittrakarn *et al.,* Rep. Pract. Oncol. Radiother. **25** (2020) 125.
30. H. Ouhadda, M. Zerfaoui, K. Bahhous *et al.,* Nucl. Anal. **3** (2024) 100112.
31. N. Arbor, J. Gasteuil, C. Noblet *et al.,* Physica Med. **61** (2019) 112.
32. I. Antcheva, M. Ballintijn, B. Bellenot *et al.*, Comput. Phys. Commun. **180** (2009) 2499.
33. A. Fathi, Y. Khobbaizi, S. Nabil *et al.,* Mater. Today Proc. **66** (2022) 466.
34. I. J. Das, C. W. Cheng, R. J. Watts *et al.*, Med. Phys. **35** (2008) 4186.
35. Y. A. M. Yousif, J. Gastaldo, and C. Baldock, Phys. Eng. Sci. Med. **45** (2022) 407.
36. S. V. Musolino, Health Phys. **81** (2001) 592.
37. T. K. Johnson, Health Phys. **92** (2007) 407.
38. D. A. Low, W. B. Harms, S. Mutic *et al.,* Med. Phys. **25** (1998) 656.